Theor Chem Acc (2015) 134:34
DOI 10.1007/s00214-015-1623-9

REGULAR ARTICLE

Structures, stabilities, and electronic properties of the neutral and anionic Si_nSm^{λ} ($n = 1$–9, $\lambda = 0, -1$) clusters: comparison with pure silicon clusters

Cheng-Gang Li · Li-Jun Pan · Peng Shao · Li-Ping Ding · Hai-Tao Feng · Dao-Bin Luo · Bo Liu

Received: 23 October 2014 / Accepted: 20 January 2015 / Published online: 25 February 2015

Abstract Geometric structures, stabilities, and electronic properties of Si_{n+1}^{λ} and Si_nSm^{λ} ($n = 1$–9, $\lambda = 0, -1$) clusters have been investigated systematically using density functional method at four levels. Extensive searches for ground state structures were carried out by the comparison between simulated spectra and the measured photoelectron spectroscopy. The results show that Sm atom tends to occupy the low-coordinated position and edge-cap or face-cap on the silicon frames. The lowest energy structures of $Si_nSm^{0/-}$ favor planar structures for $n = 1$–3 and three-dimensional structures for $n = 4$–9. Based on the averaged binding energies and fragmentation energies, we predict that Si_4Sm and Si_2Sm^- clusters have the higher relative stabilities. Furthermore, the patterns of HOMOs and derivatives of ρ for the most stable doped isomers are investigated to gain insight into the nature of bonding. The result shows that π-type or σ-type bonds are always formed among the Si atoms, and the interaction between the Sm and Si atoms is very weak. To achieve a deep insight into localization of charge and reliable charge-transfer information, the Mulliken population are analyzed and discussed. In addition, the electrostatic potential, which is well established as a guide to the interpretation and prediction of molecular behavior, is performed for the lowest energy structures of Si_nSm^{λ} ($n = 1$–9, $\lambda = 0, -1$) clusters.

Keywords Si–Sm cluster · Ground state structure · Photoelectron spectra · Electrostatic potential

1 Introduction

Silicon is the most important material for the semiconductor industry, with continuous miniaturization of the semiconductor devices. The properties of silicon-based clusters have attracted a great number of attentions. Particularly, the metal–silicon clusters have been extensively studied by both experimental [1–7] and theoretical [8–20] work, because the addition of "impurity" atoms can significantly alter their properties. For example, the notion of altering the electronic properties of silicon by doping group III (Ga, Al) and group V (P, As) elements into it has been in use for over half a century and has led to the revolutionary rise of modern computers.

Doping with transition metal atoms with unfilled *d*-shells is a promising approach to create clusters with new magnetic properties. Namely, unpaired *d*-electrons of TM (transition metal) atoms are envisioned as retaining their magnetic moments once encapsulated within a silicon cage. They might be able to serve as transitional materials between current silicon-based semiconductor technology and the nascent field of spintronics. To achieve

Electronic supplementary material The online version of this article (doi:10.1007/s00214-015-1623-9) contains supplementary material, which is available to authorized users.

C.-G. Li (✉) · L.-J. Pan (✉)
College of Physics and Electronic Engineering, Quantum Materials Research Center, Zhengzhou Normal University, Zhengzhou 450044, China
e-mail: scu_jiajia@163.com

L.-J. Pan
e-mail: zznu_lcg@163.com

P. Shao (✉) · H.-T. Feng · D.-B. Luo · B. Liu
College of Science, Shaanxi University of Science and Technology, Xi'an 710021, China
e-mail: scu_sp@163.com

L.-P. Ding
Institute of Atomic and Molecular Physics, Sichuan University, Chengdu 610065, China

this goal, several combined experimental spectrometric and theoretical studies have been carried out on doped silicon clusters Si_nM with M = V, Mn, Ti, Cr, Mo, W, and Cu [1, 21–27]. In addition, our group has investigated the structures, stabilities, and electronic properties of Cu_2Si_n [28] and Ag_2Si_n clusters [29]. However, a considerable amount of evidence shows that silicon's *sp*-orbitals interact strongly with the *d*-orbitals of the endohedral transition metal atom, thereby quenching the latter's magnetic moment [6, 13, 14]. Because a nonzero magnetic moment arises from unpaired electrons and the stability of cluster relies heavily on its ability to attain a closed shell, it becomes apparent why these two essential requirements for a magnetic cluster-assembled material are mutually exclusive when the same electrons are responsible for both bonding and magnetism.

To bypass this constraint, Khanna and Jena first proposed the endohedral doping of silicon clusters with lanthanide (Ln) atoms. It is well known that these elements have the more localized *f*-electrons. These electrons are to a large extent which is not responsible for bonding. Lanthanide atoms with multiple unpaired *f*-electrons may retain a significant portion of their atomic magnetic moments even in the presence of a strongly interacting environment such as a silicon cage. Therefore, $LnSi_n$ clusters can be easily used to study magnetic properties [30] and interest in their potential applications spurred considerable activity over the past couple of years. Ohara et al. [31, 32] have previously reported experimental photoelectron spectra and water reactivities of $TbSi_n^-$ ($6 \le n \le 16$). Kumar et al. [33] theoretically studied encapsulated fullerene-like neutral and anionic clusters, $M@Si_{20}$ (M = La, Ac, Sm, Gd, Tm, Ce, Pa, Pu, Th, Np, Pm), and observed that $Pa@Si_{20}$, $Sm@Si_{20}$, $Pu@Si_{20}$, $Tm@Si_{20}$, and $Gd@Si_{20}^-$ retain rather significant magnetic moments in their most stable geometries. Bowen's group have published the results of their experimental photoelectron spectroscopic studies of $EuSi_n^-$ ($3 \le n \le 7$) [30] and $LnSi_n^-$ (Ln = Yb, Eu, Sm, Gd, Ho, Pr; $3 \le n \le 13$) [34] anionic clusters, thereby expanding the range of studied Ln-silicon systems to encompass half of the lanthanide series. However, the literature existed on lanthanide-containing silicon clusters is still limited.

In this paper, we reported an extensive and systematical density functional theory (DFT) investigation on the small-sized neutral and anionic Si_nSm^{λ} (n = 1–9, $\lambda = 0, -1$) clusters. The pure silicon clusters were also studied by using identical methods and basis sets for comparison. The main objective of this research is to investigate the nature of interaction between silicon and samarium atoms. The various ground state minimum structures for Si_nSm^{λ} (n = 1–9, $\lambda = 0, -1$) are also obtained, which can provide significant help for such kind of cluster assemble materials.

2 Computational Methods

Geometrical structures' optimizations and frequency analysis of Si_nSm^{λ} (n = 1–9, $\lambda = 0, -1$) clusters have been performed by the DFT method using the *GAUSSIAN 03* program [35]. B3LYP density functional, which is Becke's three-parameter functional [36] (B3) in conjunction with the correlation functional of Lee, Yang, and Parr (LYP) [37], was first employed for studying this system. Afterwards, all of the obtained isomers were re-optimized and their relative energies for the different isomers in a cluster were re-calculated using XC-M06 method. Furthermore, a selected set of the low-energy optimized structures was tested by B3PW91 [36, 38–40] and CCSD (t) [41–43] methods. This can guarantee the accuracy of our calculations. The basis sets labeled GENECP are the combination of 6-311 + G* [44] and MWB52 basis sets, which are employed for the Si and Sm atom, respectively. The ECP of MWB52 was developed by Dolg et al. [45, 46] for lanthanide metal atoms. A total of $46 + 4f^6$ electrons are included in the lanthanide core, and the remaining 10 electrons are treated explicitly. Moreover, the adiabatic detachment energies (ADEs) were calculated using B3LYP, B3PW91, and CCSD (t) methods. The results comparing with experimental values [34] are presented in Table 1.

In this paper, the equilibrium geometries of pure silicon clusters were first studied based on the previous investigations. The pure silicon clusters in the range of 2–10 atoms have been well studied [47–51], and our obtained structures agree well with the previous results [47, 49]. To search for the lowest energy structure of Si_nSm^{λ} clusters, a large number of initial structures were obtained by placing the Sm atom on each possible site of the $Si_n^{0/-}$ host clusters as well as by substituting one Si atom using Sm in $Si_{n+1}^{0/-}$ clusters. The previous studies [52, 53] on other lanthanide atoms doped silicon clusters are also employed as a guide. Due to the spin polarization, every initial structure is optimized at various possible spin multiplicities. In order to select most likely candidate structures, we have performed the simulated photoelectron spectroscopy (PES) spectra for obtained isomers and compared them with Bowen's experimental spectra [34]. As is well known, well-resolved experimental PES spectra serve as electronic "fingerprints" of the underlying clusters.

3 Results and discussion

3.1 Geometrical structures

Based on the method that has been pointed out above, a large number of optimized isomers for Si_nSm^{λ} (n = 1–9, $\lambda = 0, -1$) clusters are obtained. We select the four most

Table 1 Electronic states, symmetries, relative energies (ΔE), HOMO energies, and LUMO energies of Si_{n+1}^{λ} and Si_nSm^{λ} ($n = 2$–9; $\lambda = 0, -1$) clusters

Isomer	State	Sym.	ΔE (eV)	HOMO (eV)	LUMO (eV)	Isomer	State	Sym.	ΔE (eV)	HOMO (eV)	LUMO (eV)
Si_3	$^3A_1$	D_{3h}	–	−6.249	−4.111	Si_3^-	$^2A'$	C_{2v}	–	−0.545	1.123
2N-a	$^1A_1$	C_{2v}	0.00	−4.451	−2.908	2A-a	$^2A_1$	C_{2v}	0.00	−0.256	1.113
2N-b	$^1A_1$	$C_{\infty v}$	0.28	−4.313	−3.115	2A-b	$^2\Sigma_g$	$C_{\infty v}$	0.12	−0.435	2.800
2N-c	$^3A_1$	C_{2v}	0.30	−4.15	−3.26	2A-c	$^4B_2$	C_{2v}	1.36	−0.173	0.729
2N-d	$^5\Sigma_g$	$D_{\infty h}$	2.92	−4.98	−3.87	2A-d	$^6B_2$	C_{2v}	2.06	−0.972	1.268
Si_4	^1A_g	D_{2h}	–	−6.229	−3.805	Si_4^-	$^2B_{2g}$	D_{2h}	–	−0.416	1.384
3N-a	^1A	C_{2v}	0.00	−4.449	−3.329	3A-a	$^2A_1$	C_s	0.00	−0.567	0.669
3N-b	$^1A_1$	C_{2v}	0.51	−0.291	1.055	3A-b	$^2A'$	C_s	0.13	−0.661	0.662
3 N-c	$^1A_1$	C_{3v}	0.89	−4.068	−3.185	3A-c	^4A	C_s	1.24	0.095	0.666
3N-d	$^1A_1$	C_{2v}	4.48	−4.757	−4.556	3A-d	^4A	C_{2v}	1.86	−1.226	0.388
Si_5	$^1A_1'$	D_{3h}	–	−6.373	−3.203	Si_5^-	$^2A_2''$	D_{2h}	–	−1.446	0.446
4N-a	$^1A'$	C_s	0.00	−4.580	−3.028	4A-a	$^2A''$	C_s	0.00	−0.862	0.939
4N-b	$^3A''$	C_s	0.26	−4.168	−1.858	4A-b	$^2A_1$	C_{2v}	0.58	−0.576	0.173
4N-c	^1A	C_s	0.47	−4.495	−3.158	4A-c	$^4A_2$	C_{2v}	0.92	−0.257	0.391
4N-d	$^3B_2$	C_{2v}	0.48	−4.610	−2.075	4A-d	^4A	C_s	1.33	−0.182	0.441
Si_6	$^1A_1'$	C_{2v}	–	−6.230	−3.018	Si_6^-	$^2A_{2u}$	D_{4h}	–	−1.181	0.674
5N-a	$^1A'$	C_s	0.00	−4.842	−3.226	5A-a	$^1A'$	C_s	0.00	−0.866	0.268
5N-b	$^1A'$	C_s	0.16	−4.727	−2.569	5A-b	$^2A'$	C_s	0.14	−0.935	0.112
5N-c	$^3B_1$	C_{2v}	0.21	−4.461	−1.637	5A-c	$^4A_1$	C_{4v}	0.95	−0.628	0.552
5N-d	^1A	C_{3v}	0.39	−4.825	−3.220	5A-d	$^4A_2$	C_{2v}	1.34	−0.835	0.123
Si_7	$^1A_1'$	D_{5h}	–	−6.356	−3.192	Si_7^-	$^2A_2''$	D_{4h}	–	−0.851	0.794
6N-a	$^1A'$	C_s	0.00	−4.371	−2.862	6A-a	$^2A'$	C_{2v}	0.00	−0.863	0.289
6N-b	$^3B_2$	C_{2v}	0.05	−4.549	−2.246	6A-b	$^2A'$	C_s	0.07	−0.953	0.331
6N-c	$^1A'$	C_s	0.10	−4.645	−3.015	6A-c	$^2B_1$	C_{2v}	0.15	−0.997	0.384
6N-d	$^3B_1$	C_{2v}	0.32	−4.529	−1.823	6A-d	$^2A'$	C_s	0.59	−1.133	0.364
Si_8	^1A_g	C_{2h}	–	−5.786	−3.202	Si_8^-	^2B_u	C_{2h}	–	−1.139	0.326
7N-a	^1A	C_s	0.00	−4.148	−3.038	7A-a	$^2A''$	C_s	0.00	−1.070	0.016
7N-b	$^3B_1$	C_{2v}	0.05	−4.274	−1.802	7A-b	^2A	C_1	0.28	−0.840	0.221
7N-c	^1A	C_1	0.11	−4.774	−3.179	7A-c	$^2A'$	C_s	0.54	−0.819	0.420
7N-d	$^1A'$	C_s	0.38	−4.497	−3.014	7A-d	$^2A'$	C_s	0.59	−0.885	0.385
Si_9	$^1A'$	C_s	–	−6.151	−3.256	Si_9^-	$^2A'$	C_s	–	−1.228	0.187
8N-a	$^1A'$	C_s	0.00	−4.749	−3.739	8A-a	$^2A'$	C_s	0.00	−1.404	−0.164
8N-b	^3B	C_2	0.12	−4.612	−2.213	8A-b	$^2A'$	C_s	0.70	−1.252	−0.081
8N-c	^1A	C_1	0.23	−4.900	−2.891	8A-c	$^2A'$	C_s	0.81	−1.133	−0.018
8N-d	^1A	C_1	0.31	−4.768	−3.136	8A-d	^2A	C_s	0.95	−1.208	0.387
Si_{10}	^1A	C_{3v}	–	−6.495	−3.477	Si_{10}^-	^2A	C_{3v}	–	−1.295	−0.056
9N-a	^1A	C_1	0.00	−4.780	−3.031	9A-a	^2A	C_{3v}	0.00	−1.669	−0.621
9N-b	^1A	C_1	0.19	−4.678	−3.091	9A-b	$^2A'$	C_s	0.12	−1.410	−0.111
9N-c	$^1A'$	C_s	0.26	−4.633	−2.991	9A-c	$^2A'$	C_s	0.22	−1.506	−0.273
9N-d	$^1A'$	C_s	0.34	−4.452	−3.048	9A-d	$^2A'$	C_s	0.42	−1.067	−0.006

likely candidate isomers for each size and list them in Figs. 1, 2, and 3. According to their energies from low to high, the neutral isomers are designated by *n*N-a, *n*N-b, *n*N-c, and *n*N-d; the anions are designated by *n*A-a, *n*A-b, *n*A-c, and *n*A-d, where *n* represents the number of Si atoms in $Si_nSm^{0/-}$ clusters. In order to examine the effects of dopant Sm atom in silicon clusters, geometry optimizations of $Si_n^{0/-}$ ($n = 2$–10) clusters have been carried out using the identical method and basis set, and the lowest energy structures are also displayed for comparison. The corresponding relative energies, symmetries, electronic states, highest occupied molecular orbital (HOMO) energies, and

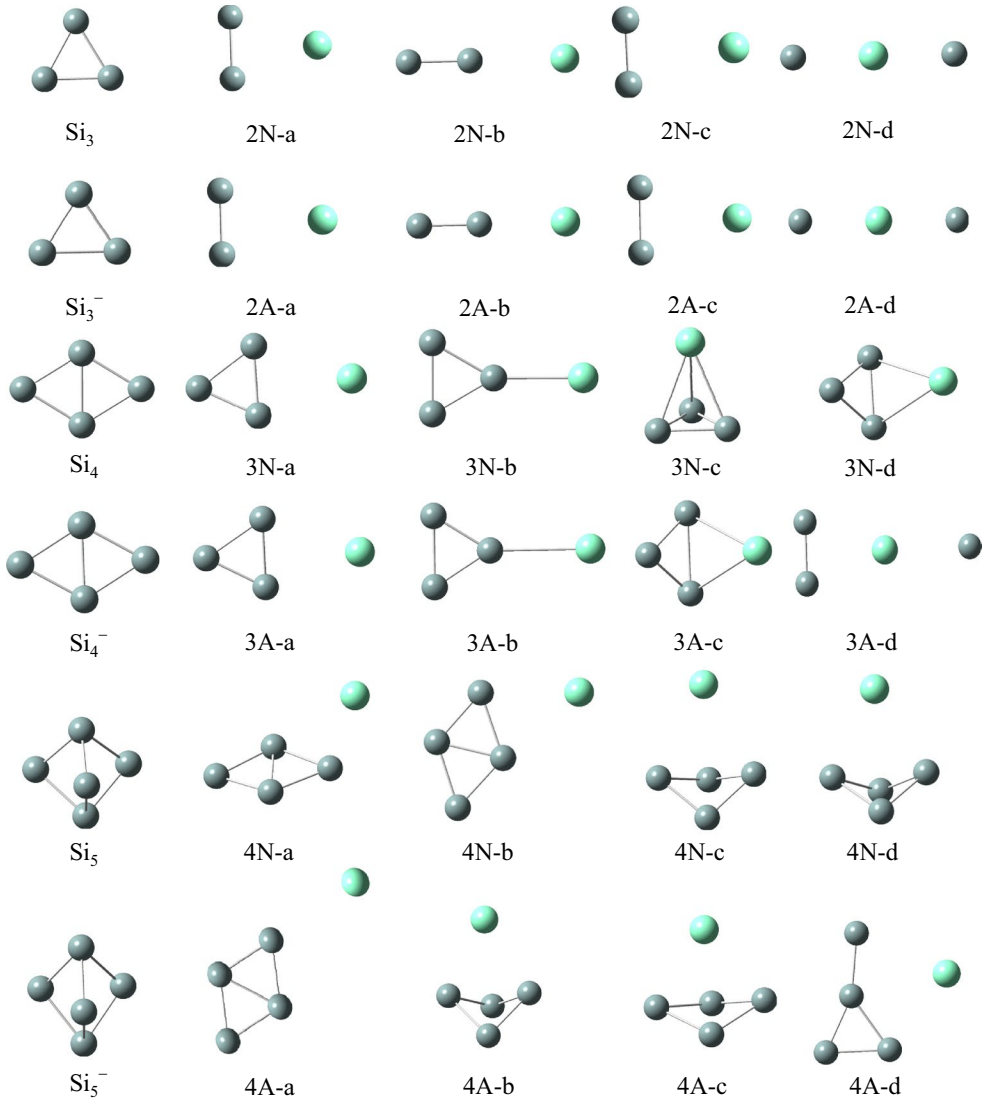

Fig. 1 Ground state structures of Si_{n+1}^{λ} and Si_nSm^{λ} ($n = 2$–4; $\lambda = 0, -1$) clusters, and some low-lying isomers for doped clusters

LUMO energies for the selected pure and doped clusters are summarized in Table 2. Furthermore, the energetically low-lying isomers optimized at M06 XC level are shown in supplementary material (Fig. S1, S2, and S3) to verify our geometries.

3.1.1 Bare silicon clusters $Si_n^{0/-}$ ($n = 2$–10)

As shown in Figs. 1, 2, and 3, our ground state structures of Si_n and Si_n^- ($n = 2$–10) clusters are in good agreement with the isomers reported in previous studies [47, 54, 55]. For the smallest clusters Si_2 and Si_2^-, the ground states are calculated to be $^3\Sigma_g$ and $^2\Sigma_g$, respectively. Their bond lengths are calculated to be (2.253, 2.187), (2.281, 2.197), and (2.271, 2.190) at CCSD (t), B3LYP, and B3PW91 levels. These results agree well with the experimental studies. The Si_2 has an experimental bond length 2.246 Å [54, 55], and the experimental bond length of Si_2^- is 2.127 as given by Nimlos et al. [54]. The ground state structures of both neutral and anionic $Si_n^{0/-}$ clusters change from planar to three-dimensional (3D) structure at $n = 5$. The studied neutral and anionic silicon clusters tend to have the similar structures except for $n = 6$, and almost all of them have high symmetry.

3.1.2 Si_nSm^{λ} ($n = 1$–9, $\lambda = 0, -1$) clusters

The B3LYP density functional was first employed for studying this system. Henceforth, the values of bond length and relative energies are given at B3LYP level, unless

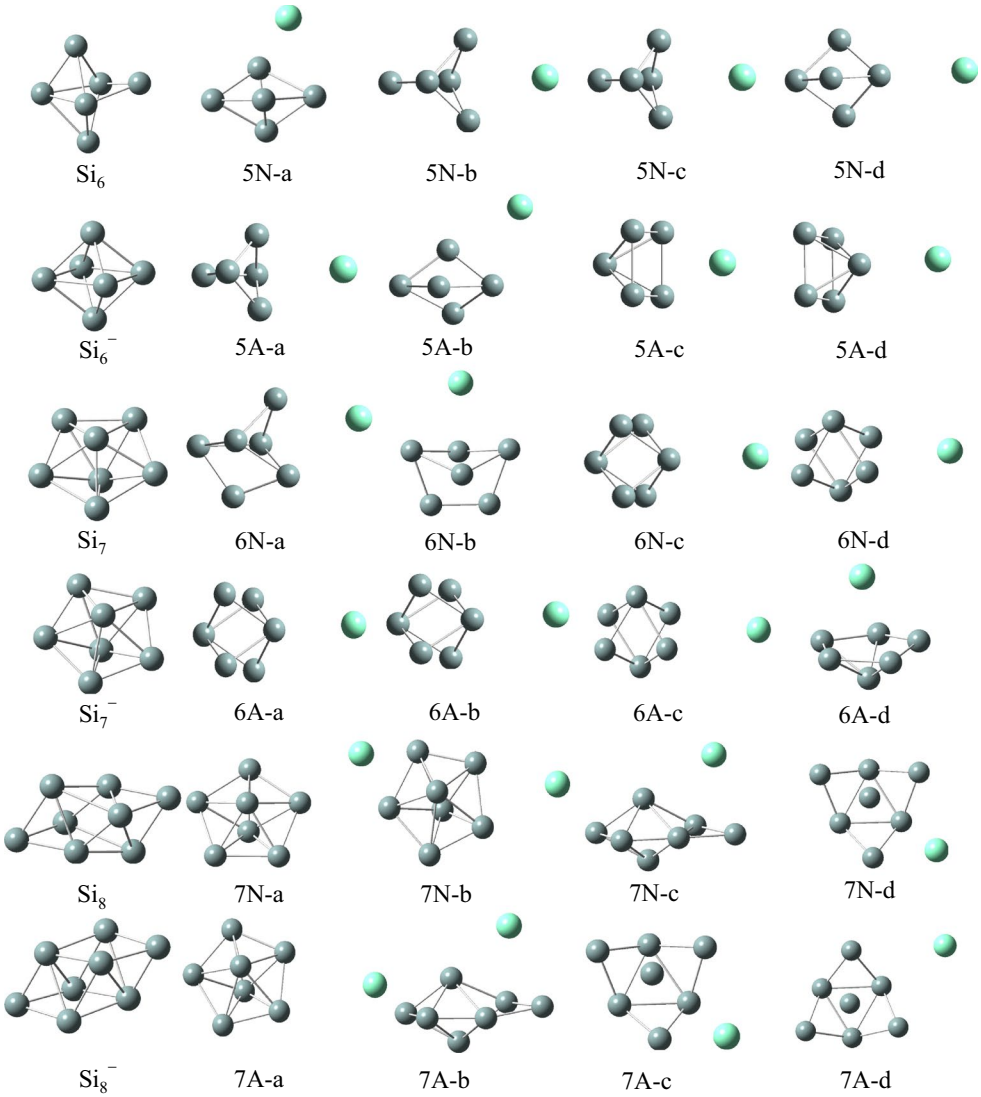

Fig. 2 Ground state structures of Si_{n+1}^{λ} and Si_nSm^{λ} ($n = 5$–7; $\lambda = 0, -1$) clusters, and some low-lying isomers for doped clusters

mentioned otherwise. At B3LYP level, our obtained ground state of SiSm is shown to be $^1\Sigma$, with 3.387 Å bond length. Upon an extra electron attachment, the ground state of anion $SiSm^-$ will change to be $^2\Sigma$, and the bond length is shortened to 3.355 Å. Unfortunately, there are no experimental and theoretical results for the smallest $SiSm^{0/-}$ monomer available. Our theoretical results need to be further verified by experiments. All possible initial structures of $Si_2Sm^{0/-}$ clusters, i.e., linear structures ($D_{\infty h}$, $C_{\infty v}$), and triangle structures (acute angle or obtuse angle) are optimized with the different spin multiplicities. The triangle structures (2 N-a and 2A-a) with acute angle are found to be the most stable isomers for neutral and anionic clusters. Both of them can be obtained by replacing one Si atom by Sm in the corresponding ground state $Si_3^{0/-}$ clusters. Furthermore, the lowest energy isomer of 3 N-a and 3A-a can also be derived from ground state $Si_4^{0/-}$ clusters by this method.

Moving on to the next bigger cluster, we found that the lowest energy structure for $Si_4Sm^{0/-}$ (Fig. 1) begin to show 3D appearance with C_s symmetry. They can be seen as Si_4 clusters capped by a Sm atom. When the number of silicon atoms is up to 5, no low-lying planar structure is found in our calculations. For Si_6Sm, as shown in Fig. 2, it can be seen that the lowest energy has C_s symmetry with $^1A'$ state, while the ground state structures of Si_6Sm^- has C_{2v} symmetry and $^2A'$ electronic state. Both of the lowest energy structures of neutral and anionic Si_7Sm have C_s symmetry, and they can be obtained by adding one Si atom on the $Si_7^{0/-}$ clusters. For $Si_8Sm^{0/-}$ clusters, when the top Si atom of the ground state structure for $Si_9^{0/-}$ is substituted by a Sm atom, their ground state structures can be obtained. As shown in Fig. 3, we showed four low-energy isomers for $Si_9Sm^{0/-}$, respectively. All of them have the Sm atom face-capped on silicon clusters. According to the above discussions, we discuss the general features observed in

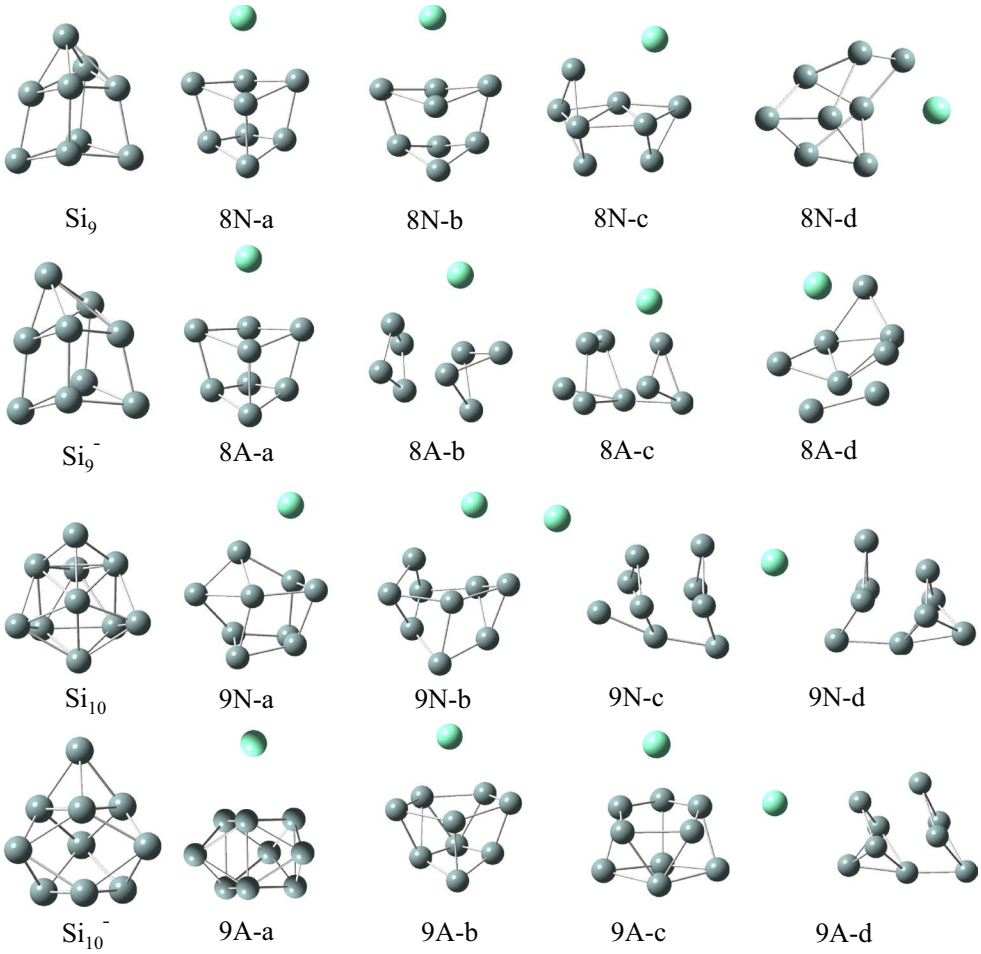

Fig. 3 Ground state structures of Si_{n+1}^{λ} and Si_nSm^{λ} ($n = 8$–9; $\lambda = 0, -1$) clusters, and some low-lying isomers for doped clusters

Table 2 Calculated adiabatic electron affinities of Si_nSm^{λ} ($n = 2$–9; $\lambda = 0, -1$) compared to experimental values

AEA (eV)	Methods				
	Exp.[a]	CCSD (T)	B3PW91	B3LYP	M06
Si_2Sm		0.93	1.57	1.57	1.66
Si_3Sm	1.40 ± 0.05	1.31	1.99	1.94	2.01
Si_4Sm	1.50 ± 0.05	1.36	1.89	1.84	1.82
Si_5Sm	1.60 ± 0.05	1.76	2.10	2.05	2.07
Si_6Sm	1.50 ± 0.10	1.67	2.07	1.98	2.11
Si_7Sm	1.60 ± 0.10	1.73	2.12	2.07	1.83
Si_8Sm	2.60 ± 0.20	2.64	2.59	2.58	2.34
Si_9Sm	2.10 ± 0.10	2.25	2.43	2.13	2.40

these clusters. Starting at $n = 4$, the lowest energy structures of neutral and anionic doped clusters begin to show appearance of 3D geometries. The ground state structures of neutral and anionic $Si_nSm^{0/-}$ clusters have the similar structures except for $n = 5$, 6, and 9. The Sm atom tends to occupy the low-coordinated position and edge-cap or face-cap on the silicon clusters.

3.2 Comparison between the simulated PES spectra and the measured spectra

A PES experiment on Si_nSm^- ($n = 3$–13) was carried out using a magnetic-bottle time-of-flight photoelectron spectrometer equipped with a laser vaporization cluster source by Bowen's group [34]. As we all know, well-resolved PES spectra serve as electronic "fingerprints" of the underlying clusters and can be used for comparisons with theoretical simulations. In this case, we have performed the simulated spectra by adding the relative energies of the orbitals ($\Delta E_n = E_{(\mathrm{HOMO}\text{-}n)} - E_{\mathrm{HOMO}}$) to the VDE, and then, they are fitted with a unit-area Gaussian function of 0.2 eV full width at half maximum. The VDEs of each cluster anion correspond to the first peak maximum of each spectrum in Fig. 4. Due to the nonadiabatic interactions and anharmonic resonances are not included during our calculations, it is not possible to quantitatively compare calculated intensities with experimental ones, but the positions and the general shape of the peaks overall agree with experimental spectra. As can be seen in Fig. 4, the numbers of distinct peaks of simulated photoelectron spectra in the low-binding-energy

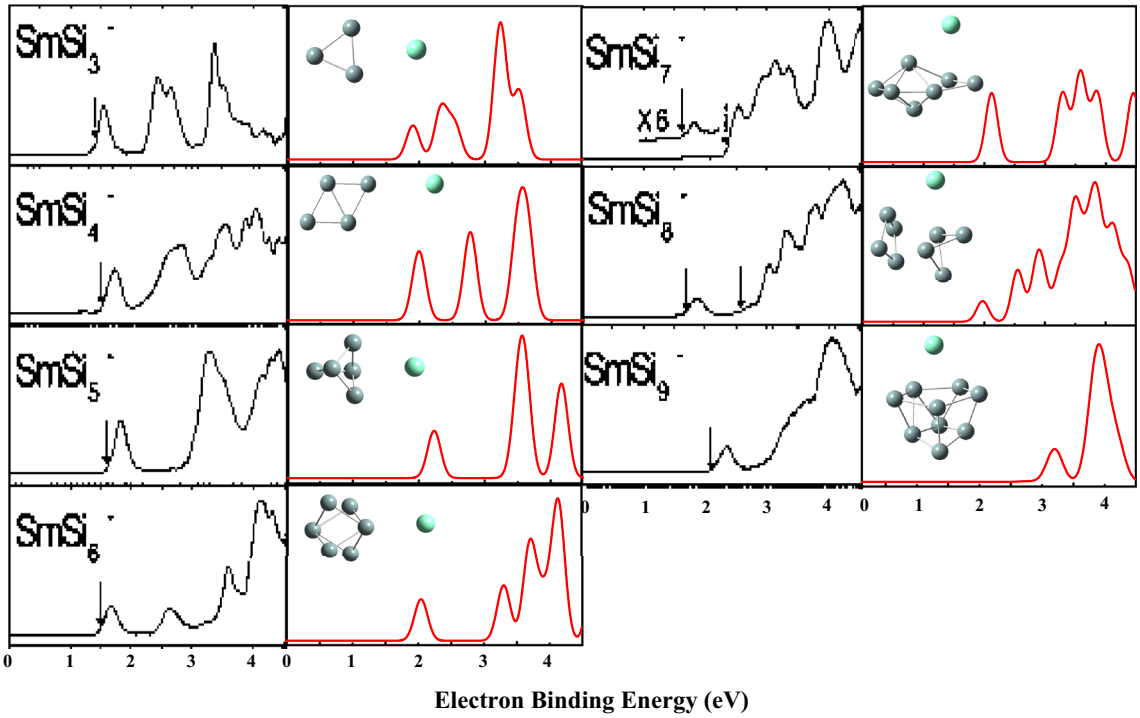

Fig. 4 Photoelectron spectra of Si_nSm^- ($n = 3$–9) measured at 266 nm (The spectra are taken from Ref. [36]. Copyright 2009 American Chemical Society). Simulated photoelectron spectra for the lowest energy structures of Si_nSm^- ($n = 3$–9) clusters at the B3LYP level

range of ≤4.5 eV and their relative positions overall agree with the experimental spectra. Those increase the confidence in the reliability of the ground state structure isomers obtained.

3.3 Relative stabilities

In order to investigate the relative stabilities of the ground state Si_nSm^{λ} ($n = 1$–9, $\lambda = 0, -1$) clusters, we have calculated the averaged binding energies $E_b(n)$ and fragmentation energies $\Delta E(n)$. Considering the influence of impurity atom on the small pure clusters, all of the above calculations are compared with the pure Si_{n+1}^{λ} ($n = 1$–9, $\lambda = 0, -1$) clusters. For Si_nSm^{λ} ($\lambda = 0, -1$) clusters, $E_b(n)$ and $\Delta E(n)$ are defined as the following formula:

$$E_b(n) = \left[E(\mathrm{Si}^{\lambda}) + (n-1)E(\mathrm{Si}) + E(\mathrm{Sm}) - E(\mathrm{Si}_n\mathrm{Sm}^{\lambda})\right] \Big/ (n+1) \quad (1)$$

$$\Delta E(n) = E(\mathrm{Si}_{n-1}\mathrm{Sm}^{\lambda}) + E(\mathrm{Si}) - E(\mathrm{Si}_n\mathrm{Sm}^{\lambda}) \quad (2)$$

where $E(\mathrm{Si})$, $E(\mathrm{Si}^{\lambda})$, $E(\mathrm{Si}_n\mathrm{Sm}^{\lambda})$, and $E(\mathrm{Si}_{n-1}\mathrm{Sm}^{\lambda})$ denote the total energies of Si, Sm^{λ}, $\mathrm{Si}_n\mathrm{Sm}^{\lambda}$, and $\mathrm{Si}_{n-1}\mathrm{Sm}^{\lambda}$ clusters, respectively.

For Si_{n+1}^{λ} ($\lambda = 0, -1$) clusters, $E_b(n)$ and $\Delta E(n)$ are defined as follows:

$$E_b(n+1) = \left[E\left(\mathrm{Si}^{\lambda}\right) + nE(\mathrm{Si}) - E\left(\mathrm{Si}_{n+1}^{\lambda}\right)\right] \Big/ (n+1) \quad (3)$$

$$\Delta E(n+1) = E\left(\mathrm{Si}_n^{\lambda}\right) + E(\mathrm{Si}) - E\left(\mathrm{Si}_{n+1}^{\lambda}\right) \quad (4)$$

where $E(\mathrm{Si})$, $E(\mathrm{Si}^{\lambda})$, $E(\mathrm{Si}_n^{\lambda})$, and $E(\mathrm{Si}_{n+1}^{\lambda})$ denote the total energies of Si, Si^{λ}, Si_n^{λ}, and $\mathrm{Si}_{n+1}^{\lambda}$ clusters, respectively.

The $E_b(n)$ and $\Delta E(n)$ values of the lowest energy Si_{n+1}^{λ} and Si_nSm^{λ} ($n = 1$–9, $\lambda = 0, -1$) clusters against the corresponding number of the Si atoms are plotted in Fig. 5. The features of size evolution are best viewed, and the peaks of curves correspond to those clusters with enhanced local stabilities. For pure Si_{n+1} and Si_{n+1}^- clusters, the averaged binding energies increase gradually with the cluster size increasing at $n \leq 5$; then, the curves become to slow down. The curve of Si_{n+1}^- is higher than that of the corresponding sized Si_{n+1} clusters, reflecting that the stability is enhanced when the cluster attach an extra electron. The dissociation energies of Si_2, Si_2^-, SiSm, and $SiSm^-$ dimers are 3.065, 3.829, 0.641, and 0.395 eV, respectively. These reflect that the Si–Si interaction is much stronger than that of Si–Sm. For both $E_b(n)$ and $\Delta E(n)$ curves, the visible peak occurs at Si_4 and Si_{10}^-, hinting that they are more stable than their neighboring clusters.

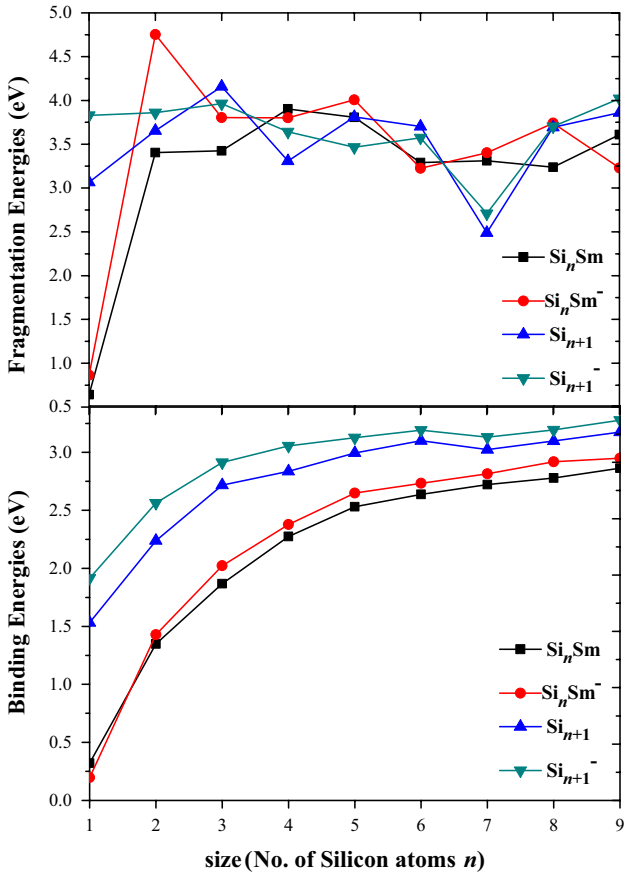

Fig. 5 Size dependence of the averaged binding energies $E_b(n)$ and fragmentation energies $\Delta E(n)$ for the ground state structures of Si_{n+1}^{λ} and Si_nSm^{λ} ($n = 1$–9; $\lambda = 0, -1$) clusters

For Si_nSm^{λ} ($n = 1$–9, $\lambda = 0, -1$) clusters, the averaged binding energies are lower than those of the corresponding sized pure silicon clusters, reflecting that the stability of $Si_n^{0/-}$ clusters cannot be enhanced when Sm atom is doped into them. The two curves increase gradually with the cluster size increasing for the entire size. Fragmentation energy involves the energy that a Si atom is separated from $Si_nSm^{0/-}$ clusters. Two conspicuous maxima are found at Si_4Sm and Si_2Sm^-. Accordingly, this indicates that Si_4Sm and Si_2Sm^- clusters are the most stable clusters in their respective species.

3.4 Orbital and bonding properties analysis

The highest occupied–lowest unoccupied molecular orbital (HOMO–LUMO) energy gap, which represents the ability of molecule to participate into chemical reaction in some degree, has been examined. In a sense, it can provide an important criterion to reflect the chemical stability of clusters. A large value of the HOMO–LUMO energy gap is related to an enhanced chemical stability. In contrast, a small one corresponds to a high chemical activity. For the most stable Si_{n+1}^{λ} and Si_nSm^{λ} ($n = 1$–9, $\lambda = 0, -1$) clusters, HOMO and LUMO energies are listed in Table 1. In addition, the HOMO–LUMO energy gaps against the cluster size are also plotted in Fig. 6. As shown in Fig. 6, there are no apparent odd–even alternation behaviors in the four curves, but they show very irregular behaviors. The HOMO–LUMO energy gaps of pure Si_{n+1} clusters show the same tendency with our previous results [28]. For Si_nSm and Si_nSm^- clusters, the remarkable peaks occur at Si_9Sm, $SiSm^-$, and Si_4Sm^- clusters, which imply that these clusters have the larger HOMO–LUMO gaps than others and possess dramatically enhanced chemical stability. For Si_8Sm cluster, the gap is very small compared to the neighbor's, indicating that the chemical activity of Si_8Sm is stronger than that of its neighboring clusters.

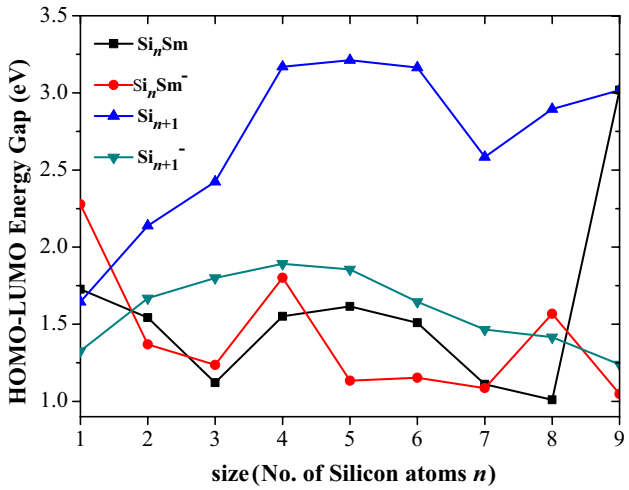

Fig. 6 Size dependence of the HOMO–LUMO energy gaps of the ground state Si_{n+1}^{λ} and Si_nSm^{λ} ($n = 1$–9; $\lambda = 0, -1$) clusters

In order to gain insight into the nature of the bonding, we have analyzed the HOMO for the most stable $Si_nSm^{0/-}$ clusters. The patterns of HOMOs are displayed in Fig. 7. These MOs provide insight into the observed special features and the nature of bonding in Sm-doped and pure silicon clusters. In pure Si_2 dimer, we found that the π-type bond is formed between Si and Si atoms. However, when Sm substitutes one Si atom, the π-type bond disappears but with mixed Si *p* characters. Upon an electron attachment, the Sm *s* character emerges in $SiSm^-$ cluster. As for 2N-a structure, the two silicon atoms form σ_{2p}-type bond. When an electron attach to 2N-a, the σ_{2p}-type bond is changed to be π-type bond but with mixed Sm-*s* character. Across all the HOMOs of the most stable $Si_nSm^{0/-}$ clusters, the π-type or σ-type bonds are always formed among the Si atoms. In some clusters, the Sm atoms form σ bonding through an overlap between vacant in-plane Si *p* orbitals and valence Sm *s* orbitals. In the other clusters, the Sm

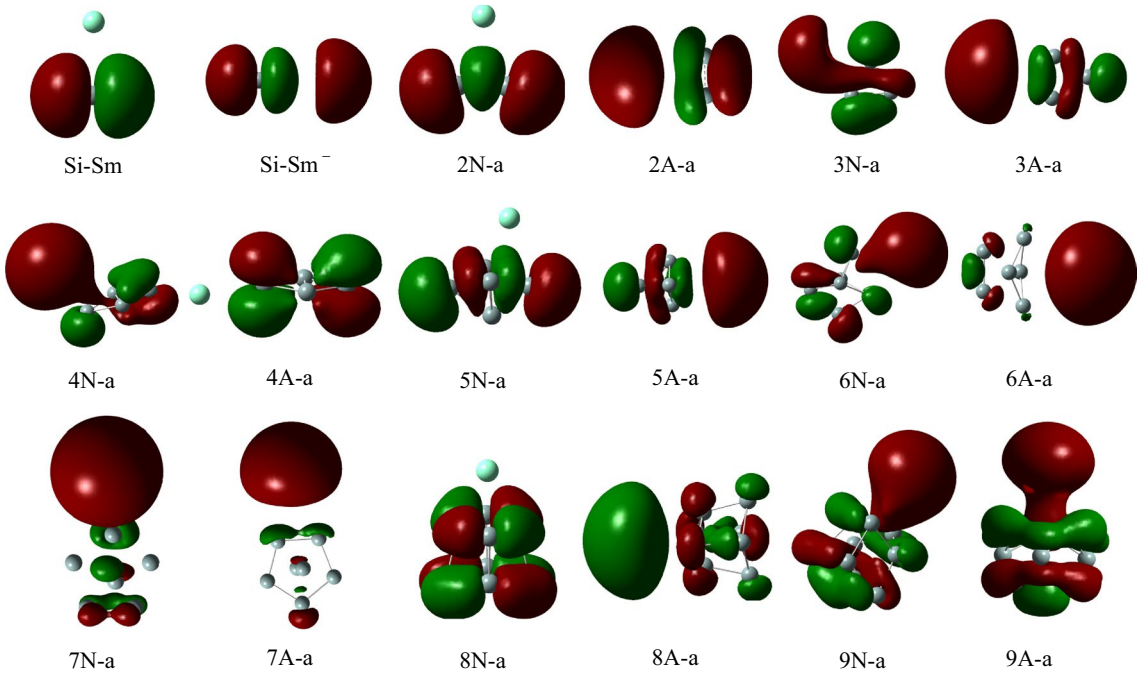

Fig. 7 Contour maps of the HOMOs of the ground state Si_nSm^{λ} ($n = 1$–9; $\lambda = 0, -1$) clusters

Table 3 Electron density [$\rho(r_{BCP})$], Laplacian [$\nabla^2\rho(r_{BCP})$], bond ellipticity (ε), and curvature λ_3 at bond critical points of the ground state of neutral and anionic $Si_nSm^{0/-}$ ($n = 1$–9) clusters

n	BCP	ρ	$\nabla^2\rho\,(r_{BCP})$	ε	λ_3	n	BCP	ρ	$\nabla^2\rho\,(r_{BCP})$	ε	λ_3
SiSm	Sm–Si_1	0.012	0.024	0.000	0.034	$SiSm^-$	Sm–Si_1	0.008	0.015	0.000	0.021
Si_2Sm	Sm–Si_1	0.015	0.042	9.855	0.050	Si_2Sm^-	Sm–Si_1	0.009	0.022	2.602	0.027
Si_3Sm	Sm–Si_2	0.013	0.031	0.278	0.042	Si_3Sm^-	Sm–Si_2	0.012	0.031	0.476	0.040
	Sm–Si_3	0.011	0.025	0.986	0.033		Sm–Si_3	0.011	0.027	2.182	0.033
Si_4Sm	Sm–Si_1	0.012	0.022	0.031	0.033	Si_4Sm^-	Sm–Si_3	0.007	0.014	0.057	0.020
Si_5Sm	Sm–Si_4	0.016	0.039	0.118	0.052	Si_5Sm^-	Sm–Si_1	0.013	0.032	0.440	0.042
	Sm–Si_6	0.016	0.039	0.118	0.052		Sm–Si_3	0.013	0.032	0.440	0.042
Si_6Sm	Sm–Si_3	0.012	0.022	0.118	0.032	Si_6Sm^-	Sm–Si_1	0.005	0.007	0.193	0.010
							Sm–Si_2	0.005	0.007	0.192	0.010
Si_7Sm	Sm–Si_5	0.007	0.010	0.011	0.015	Si_7Sm^-	Sm–Si_1	0.005	0.009	0.401	0.012
							Sm–Si_6	0.005	0.008	5.504	0.010
Si_8Sm	Sm–Si_6	0.015	0.047	0.068	0.058	Si_8Sm^-	Sm–Si_6	0.011	0.034	0.078	0.041
	Sm–Si_7	0.015	0.047	0.068	0.058		Sm–Si_7	0.011	0.034	0.078	0.041
Si_9Sm	Sm–Si_4	0.012	0.029	0.063	0.039	Si_9Sm^-	Sm–Si_3	0.013	0.039	0.233	0.051
	Sm–Si_8	0.016	0.032	0.078	0.047		Sm–Si_4	0.013	0.039	0.233	0.051

atoms only show *s* character or have no orbital density localized. In addition, the interaction between the Sm and Si atoms is very weak. This may be related to the electronic configuration of Sm atom that is characterized by a closed shell and two 6*s* valence electrons ($5s^2p^66s^2$), while the electronic configuration of Si atom is ($1s^22s^2p^63s^2p^2$).

To reveal the nature of chemical bonding for Si–Sm bond, we used the AIM (atoms in molecules) model to analyze the derivatives of electron density in the ground state $Si_nSm^{0/-}$ ($n = 1$–9) clusters. The electron density [$\rho(r_{BCP})$], Laplacian [$\nabla^2\rho(r_{BCP})$], bond ellipticity (ε), and curvature λ_3 at bond critical points (BCP), which contain a wealth of chemical information, are summarized in Table 3. The BCP are between Sm atom and the nearest Si atoms. The bond ellipticity is a quantity defined as $\varepsilon = (\lambda_1/\lambda_2) - 1$, where λ_i are eigenvalues of the Hessian matrix of electron density at a BCP. The Laplacian of electron density, which is the trace of the Hessian matrix of ρ, can be used as criteria to classify the interaction between atoms. When the electron density $\rho(r_{BCP})$ itself is large, and the Laplacian at

the BCP $\nabla^2\rho(r_{BCP})$ is less than zero and large in absolute value, the electron density is concentrated in the internuclear region, and the bond will be referred to as a shared interaction or covalent bond. This type of bond is always strong. In contrast, a positive Laplacian at the BCP suggests a closed-shell system. At the BCP of the closed-shell interaction, the electron density is depleted. That is to say these interactions are relatively weak. As for Si–Sm bond BCP in Table 3, we can see that the $\nabla^2\rho(r_{BCP})$ is positive, and its absolute value is small. Furthermore, the electron density is also relatively small. In this case, the interactions between Si and Sm atoms are dominated by the contraction of electronic charge away from the interatomic surface toward the nuclei and relatively weak.

3.5 Electronic properties

The Mulliken population (MP) can provide the localization of charge and reliable charge-transfer information. Here, the MP for the lowest energy species of Si_nSm^{λ} (n = 1–9, $\lambda = 0, -1$) have been calculated and summarized in Table S1 and S2, respectively. As shown in Table S1, it can be clearly seen that the samarium atoms in neutral Si_nSm clusters possess positive charges ranging from 0.139e to 1.233e, while most of the Si atoms possess negative charges. This indicates that the electron transfer from Sm atom to the Si_n frames, namely samarium atom, acts as electron donor in all the neutral clusters. This may be due to the electronegativity of Sm (1.17) that is much smaller than Si (1.98); therefore, the silicon atoms has a stronger ability to attract electrons. Even in the anionic Si_nSm^- clusters, most of the Sm atoms are still with positive charges. Only in $SiSm^-$, Si_4Sm^-, and Si_7Sm^- clusters, the Sm atoms possess −0.122e, −0.108e, and −0.106e charges, respectively.

The electrostatic potential (ESP) created by the nuclei and electrons of a molecule in the surrounding space is well established as a guide to the interpretation and prediction of molecular behavior. An important feature of the ESP is that it is a real physical property that can be determined experimentally by diffraction methods, as well as computationally. In this work, we used self-consistent-field (SCF) molecular orbital methods to compute ESP. The ESP $V(\vec{r})$ evaluated at point specified by the position vector $\vec{r}$ is given by:

$$V(\vec{r}) = \sum_A \frac{Z_A}{\left|\vec{R}_A - \vec{r}\right|} - \int \frac{\rho(\vec{r'})}{\left|\vec{r'} - \vec{r}\right|} \mathrm{d}\vec{r'} \quad (5)$$

where Z_A is the nuclear charge of atom A, $\vec{R}_A$ is the position of the nucleus of this atom, and $\rho(r')$ is the electron density as a function of the position vector r'. The equation being in atomic units with the electronic charge is taken as unity. The isosurface of ESP of the lowest energy Si_nSm^{λ} (n = 10–9, $\lambda = 0, -1$) species are displayed in Fig. S4. As we can see from Fig. S4, the transparent envelopes (contiguous envelope enclosing the molecular framework) represent the isosurface of ESP. The big and small balls represent Si and Sm atoms, respectively. As shown in indicator, red transparent envelopes represent negative potential, while the blue transparent envelopes represent positive potential. In all the neutral clusters, the color of the transparent envelopes changes gradually from red to blue. The transparent envelopes close to the Sm atom always show blue color appearance, indicating that the surrounding of Sm atom is positive potential. On the other hand, the transparent envelopes close to Si atoms always show the negative potential. These are in accord with the above charge analysis. The samarium atoms in the neutral Si_nSm clusters possess positive charges, while most of the Si atoms are with negative charges. In addition, the transparent envelopes close to the region between Si_n frame and Sm atom show white ring pattern, which correspond to the weak Si–Sm interaction. As for the anionic clusters, the whole of transparent envelopes show red color appearance, indicating that the surrounding of entire cluster is negative potential. This may be due to the attachment of the extra electron.

4 Conclusions

The geometrical structures, stabilities, and electronic properties of small pure silicon clusters Si_{n+1}^{λ} and Sm-doped silicon clusters Si_nSm^{λ} (n = 1–9, $\lambda = 0, -1$) have been investigated using DFT at four levels. All the results are summarized as follows.

1. Extensive searches for the ground state structures were carried out with the aid of comparisons between the simulated spectra and experimental PES data. The results showed that small-sized neutral and anionic silicon clusters tend to have high symmetry. For $Si_nSm^{0/-}$ clusters, the lowest energy structures favor planar structures for n = 1–3 and 3D structures for n = 4–9. The Sm atom tends to occupy the low-coordinated position and edge-cap or face-cap on the silicon clusters.
2. By calculating the averaged binding energies and fragmentation energies, the Si_4Sm and Si_2Sm^- clusters are tested to have the higher relative stabilities. The Si_9Sm, $SiSm^-$, and Si_4Sm^- clusters have the larger HOMO–LUMO gaps indicating their enhanced chemical stability. In order to gain insight into the nature of the bonding, the patterns of HOMOs and the derivatives of ρ for the most stable doped isomers are investigated. The result show that π-type or σ-type bonds are

always formed among the Si atoms, and the interaction between the Sm and Si atoms is very weak.

3. The MP results indicate that the electron transfer from Sm atom to the Si_n frames in all the neutral clusters, namely samarium atom, acts as electron donor. Correspondingly, the transparent envelopes close to the Sm atom always show blue color appearance, indicating that the ESP close to Sm atom is positive, while for the anionic clusters, the whole of transparent envelopes show red color appearance

References

1. Beck SM (1989) J Chem Phys 90:6306
2. Jaeger JB, Jaeger TD, Duncan MA (2006) J Phys Chem A 110:9310
3. Janssens E, Gruene P, Meijer G, Woste L, Lievens P, Fielicke A (2007) Phys Rev Lett 99:063401
4. Koyasu K, Atobe J, Akutsu M, Mitsui M, Nakajima A (2007) J Phys Chem A 111:42
5. Ohara M, Koyasu K, Nakajima A, Kaya K (2003) Chem Phys Lett 371:490
6. Zheng W, Nilles JM, Radisic D, Bowen KH (2005) J Chem Phys 122:071101
7. Hiura H, Miyazaki T, Kanayama T (2001) Phys Rev Lett 86:1733
8. Kumar V, Kawazoe Y (2001) Phys Rev Lett 87:045503
9. Miyazaki T, Hiura H, Kanayama T (2002) Phys Rev B 66:121403
10. Hagelberg F, Xiao C, Lester WA (2003) Phys Rev B 67:035426
11. Han JG, Shi YY (2001) Chem Phys 266:33
12. Jackson K, Nellermoe B (1996) Chem Phys Lett 254:249
13. Khanna SN, Rao BK, Jena P (2002) Phys Rev Lett 89:016803
14. Khanna SN, Rao BK, Jena P, Nayak SK (2003) Chem Phys Lett 373:433
15. Kumar V (2004) Comput Mater Sci 30:260
16. Kumar V (2006) Comput Mater Sci 35:375
17. Kumar V (2006) Comput Mater Sci 36:1
18. Kumar V, Majumder C, Kawazoe Y (2002) Chem Phys Lett 363:319
19. Reveles UJ, Khanna SN (2006) Phys Rev B 74:035435
20. Sen P, Mitas L (2003) Phys Rev B 68:155404
21. Ngan VT, Gruene P, Claes P, Janssens E, Fielicke A, Nguyen MT, Lievens P (2010) J Am Chem Soc 132:15589
22. Ngan VT, Janssens E, Claes P, Lyon JT, Fielicke A, Nguyen MT, Lievens P (2012) Chem Eur J 18:15788
23. Ngan VT, Pierloot K, Nguyen MT (2013) Phys Chem Chem Phys 15:5493
24. Claes P, Ngan VT, Haertelt M, Lyon JT, Fielicke A, Nguyen MT, Lievens P, Janssens E (2013) J Chem Phys 138:194301
25. Beck SM (1987) J Chem Phys 87:4233
26. Lau JT, Hirsch K, Klar P, Langenberg A, Lofink F, Richter R, Rittmann J, Vogel M, Zamudio-Bayer V, Möller T, Issendorff BV (2009) Phys Rev A 79:053201
27. Kong XY, Xu HG, Zheng W (2012) J Chem Phys 137:064307
28. Shao P, Kuang XY, Ding LP, Zhong MM, Wang ZH (2012) Phys B 407:4379
29. Zhao YR, Kuang XY, Wang SJ, Li YF, Lu P (2011) Z Naturforsch 66:353
30. Grubisic A, Wang HP, Ko YJ, Bowen KH (2008) J Chem Phys 129:054302
31. Ohara M, Miyajima K, Pramann A, Nakajima A, Kaya K (2002) J Phys Chem A 106:3702
32. Ohara M, Miyajima K, Pramann A, Nakajima A, Kaya K (2007) J Phys Chem A 111:10884
33. Kumar V, Singh AK, Kawazoe Y (2006) Phys Rev B 74:125411
34. Grubisic A, Ko YJ, Wang H, Bowen KH (2009) J Am Chem Soc 131:10783
35. Frisch MJ, Trucks GW, Schlegel HB, Scuseria GE, Robb MA, Cheeseman JR, Montgomery JA Jr, Vreven T, Kudin KN, Burant JC, Millam JM, Iyengar SS, Tomasi J, Barone V, Mennucci B, Cossi M, Scalmani G, Rega N, Petersson GA, Nakatsuji H, Hada M, Ehara M, Toyota K, Fukuda R, Hasegawa J, Ishida M, Nakajima T, Honda Y, Kitao O, Nakai H, Klene M, Li X, Knox JE, Hratchian HP, Cross JB, Bakken V, Adamo C, Jaramillo J, Gomperts R, Stratmann RE, Yazyev O, Austin AJ, Cammi R, Pomelli C, Ochterski JW, Ayala PY, Morokuma K, Voth GA, Salvador P, Dannenberg JJ, Zakrzewski VG, Dapprich S, Daniels AD, Strain MC, Farkas O, Malick DK, Rabuck AD, Raghavachari K, Foresman JB, Ortiz JV, Cui Q, Baboul AG, Clifford S, Cioslowski J, Stefanov B, Liu G, Liashenko A, Piskorz P, Komaromi I, Martin RL, Fox DJ, Keith T, Al-Laham MA, Peng CY, Nanayakkara A, Challacombe M, Gill PMW, Johnson B, Chen W, Wong MW, Gonzalez C, Pople JA (2004) Gaussian 03, revision E.01. Gaussian, Wallingford
36. Becke AD (1993) J Chem Phys 98:5648
37. Lee C, Yang W, Parr RG (1988) Phys Rev B 37:785
38. Perdew JP (1991) In: Ziesche P, Eschrig H (eds) Electronic structure of solids. Akademie Verlag, Berlin, pp 11–20
39. Perdew JP, Chevary JA, Vosko SH, Jackson KA, Pederson MR, Singh DJ, Fiolhais C (1992) Phys Rev B 46:6671
40. Perdew JP, Wang Y (1992) Phys Rev B 45:13244
41. Purvis GD, Bartlett RJ (1982) J Chem Phys 76:1910
42. Scuseria GE, Janssen CL, Schaefer HF III (1988) J Chem Phys 89:7382
43. Scuseria GE, Schaefer HF III (1989) J Chem Phys 90:3700
44. Krishnan R, Binkley JS, Seeger R, Pople JA (1980) J Chem Phys 72:650
45. Dolg M, Stoll H, Savin A, Preuss H (1989) Theor Chim Acta 75:173
46. Dolg M, Stoll H, Preuss H (1989) J Chem Phys 90:1730
47. Yang JC, Xu WG, Xiao WS (2005) J Mol Struct Theochem 719:89
48. Pouchan C, Bégué D, Zhang DY (2004) J Chem Phys 121:4628
49. Jackson K, Pederson MR, Porezag D, Hajnal Z, Frauenheim T (1997) Phys Rev B 55:2549
50. Binggeli N, Chelikowsky JR (1997) Phys Rev Lett 75:493
51. Kostko O, Leone SR, Duncan MA, Ahmed M (2010) J Phys Chem A 114:3176
52. Zhao GF, Sun JM, Gu YZ, Wang YX (2009) J Chem Phys 131:114312
53. Liu TG, Zhao GF, Wang YX (2011) Phys Lett A 375:1120
54. Nimlos MR, Harding BL, Ellison GB (1987) J Chem Phys 87:5116
55. Huber KP, Herzberg G (1979) Molecular spectra and molecular structure, constants of diatomic molecules, vol IV. Van Nostrand Reinhold, New York